Lateralized nodose ganglia gene expression implicates cholecystokinin receptors in interoceptive reward signaling

Author List:

Hailey F. Welch[1], Ishwarya Sankaranarayanan[1,2], Veronica M. Hong[1,2], Khadijah Mazhar[1,2], Benedict J. Kolber[1,2], Theodore J. Price[1,2], *Catherine A. Thorn[1]

Author Affiliation:

1. Department of Neuroscience, The University of Texas at Dallas, 800 W. Campbell Rd. Richardson, TX, 75080, USA
2. Center for Advanced Pain Studies, The University of Texas at Dallas, 800 W. Campbell Rd., Richardson, TX, 75080, USA

Lead Contact & Corresponding Author:

Catherine A. Thorn: catherine.thorn@utdallas.edu

Summary

The vagus nerves are important carriers of sensory information from the viscera to the central nervous system. Emerging evidence suggests that sensory signaling through the right, but not the left, vagus nerve evokes striatal dopamine release and reinforces appetitive behaviors. However, the extent to which differential gene expression within vagal sensory neurons contributes to this asymmetric reward-related signaling remains unknown. Here, we use single-cell RNA sequencing to identify genes that are differentially expressed between the left and right nodose ganglia (NG) to identify candidate genes likely to contribute to vagus-mediated reward signaling. We find that a group of neurons expressing *Chrna3* (nicotinic acetylcholine receptor subunit 3) and *Cckar* (cholecystokinin A receptor) is preferentially expressed in the right NG of both rats and mice. This result suggests that differential expression of gut-innervating nutrient sensors in NG neurons may contribute to asymmetric encoding of interoceptive rewards by the vagus nerves.

Keywords

Vagus nerve, transcriptomics, asymmetry, lateralization, interoception, cholecystokinin

INTRODUCTION

The vagus nerves transmit sensory information from the viscera, including cardiovascular, respiratory, and gastrointestinal (GI) organs, to the central nervous system to maintain homeostatic control over processes such as heart rate, respiration, and digestion (Berthoud & Neuhuber, 2000; Prescott & Liberles, 2022; Zhuo et al., 1997). The sensory neurons of the vagus nerve are situated in the jugular and nodose ganglia (NG), located near the base of the skull. These neurons detect a wide range of visceral signals including mechanical stretch and chemical stimuli and relay this information to the brainstem to mediate appropriate autonomic and behavioral responses (Capilupi et al., 2020; Maniscalco & Rinaman, 2018; Mazzone & Undem, 2016; Schwartz, 2000; Teckentrup & Kroemer, 2024).

Substantive research has revealed that sensorimotor vagal pathways are strikingly lateralized. For example, anatomical and functional evidence suggests that the right vagus nerve exerts greater influence than the left vagus nerve over the sinoatrial node of the heart, whereas the left vagus nerve exerts greater influence over the ventricles and atrioventricular node (Zandstra et al., 2021). Supporting this asymmetric organization of cardiac vagal inputs, animal studies have shown that right vagal stimulation or right vagotomy generally produce stronger effects on heart rate, while stimulation or vagotomy of the left nerve generally produce stronger effects on contractility (Ardell & Randall, 1986; Sitdikov et al., 2000; Woodbury & Woodbury, 1990; Yamakawa et al., 2014). Asymmetry has also been demonstrated in afferent vagal signaling. Stimulation of the right vagus nerve, but not the left, is seen to reinforce behavior and activate midbrain dopaminergic reward nuclei (Brougher et al., 2021), and gut-innervating vagal afferents likely play a key

role in this lateralized vagal reward-related signaling (Han et al., 2018). This work raises further questions about the cellular origins of asymmetric reward encoding by the right versus left vagus nerve.

Genetic sequencing studies of the NG in mice have revealed incredible diversity among NG cell types (Bai et al., 2019; Kupari et al., 2019; Mazzone & Undem, 2016; Prescott et al., 2020; Zhao et al., 2022). Transcription patterns of vagal neurons have been used to identify distinct subclasses of NG cells and their hypothesized sensory functions (Bai et al., 2019; Berthoud et al., 2021; Kupari et al., 2019). However, the extent to which differential gene expression contributes to the observed differential reward-related signaling in the right versus left NG remains unknown. Here, we use single-cell RNA sequencing (scRNA-seq) in rats to identify genes of interest that are differentially expressed between the left and right NG that may contribute to vagus-mediated reward signaling. As rats are a more commonly used laboratory model to investigate translational vagal therapies such as vagus nerve stimulation (VNS), we performed comprehensive genetic profiling of NG neurons in this species and compare our results to a publicly available mouse dataset of NG neurons (Buchanan et al., 2022).

Our results demonstrate that a group of neurons marked by the expression of *Chrna3* and *Cckar* is preferentially found in the right NG of both rats and mice. This finding suggests that differential expression of sensory receptors in NG neurons may contribute to asymmetric encoding of visceral reward signals by the vagus nerve, and implicates gut-innervating nutrient sensors, in particular, in the lateralized processing of interoceptive rewards.

RESULTS

Diverse mechanosensitive and chemosensitive cell types identified in rat nodose ganglia

We performed scRNA-seq on 12 replicate groups of NG cell suspensions. Each replicate group was formed by pooling the right or left NG from six male or female rats (**Figure 1A**). In all, an estimated 90,000-100,000 nuclei were prepared for sequencing. Data was quality controlled for total number of features and proportion of mitochondrial features prior to further analysis. Cells containing high levels of marker genes associated with muscle or myelin (*Myh4, Ttn, Mbp, Mpz*) and cells with low levels of the neuronal marker *Snap25* were also removed prior to clustering. The vagal ganglia in rodents contain cells from both the jugular and NG, though in our dataset, we found that very few cells expressed the jugular marker *Prdm12*. As jugular cells represented only a small fraction of our dataset, we elected to focus our analyses on putative NG neurons. Thus, cells expressing *Prdm12* were also removed prior to clustering. After quality control and filtering, 9,879 putative NG neurons were included in the subsequent analyses. Data from all replicate groups were integrated prior to clustering (Stuart et al., 2019). Cluster analysis of NG neurons then followed the standard workflow of feature selection, principal component analysis (PCA), and the Seurat Louvain algorithm-based clustering (Hao et al., 2021). This analysis identified 22 high-quality NG clusters (**Figure 1B-C**).

Prior sequencing of mouse NG has identified *Piezo2*-expressing (*Piezo2*+) putative mechanosensory cells and *Scn10a*-expressing “nociceptor-like” cells in the NG

(Kupari et al., 2019). Our data, in rats, replicate these fundamental results. We observed minimal co-expression of two sodium channel genes, *Scn10a* (encoding $Na_v1.8$) and *Scn1a* (encoding $Na_v1.1$) (**Figure 1C**). Expression of *Scn1a* typically coincided with expression of *Piezo2* and *Cntn1*, suggesting a myelinated and mechanosensory phenotype for the majority of these clusters. A smaller group of putative mechanosensory *Piezo2+* clusters was also identified in our dataset, which preferentially expressed *Scn10a* over *Scn1a*, and co-expressed *Tmem233* along with *Cntn1*. Most *Scn10a*-expressing clusters were not found to exhibit genes associated with mechanosensation, however. Rather, they co-expressed *Oprm1* (mu-1 opioid receptor) and many also co-expressed *Trpc4* (transient receptor potential channel 4), pointing to a chemosensory phenotype for the majority of *Scn10a*-expressing clusters. Approximately 20% of the cells in our dataset were sorted into putative mechanosensory clusters, while the vast majority of NG cells instead expressed putative chemosensory gene markers. Our computational results suggest that in rats, as has been shown previously in mice, there is little overlap of expression of *Scn1a* and *Scn10a* in NG neurons, and that expression of the *Scn1a* vs. *Scn10a* is highly (though not exclusively) correlated with putative mechanosensory vs. chemosensory functions, respectively.

Nodose ganglia clusters express both unique and overlapping sensory receptor transcripts

We next examined the cluster-defining transcripts for each of our 22 identified NG clusters (**Figure 2A**). Among these genes were a large number that encode

membrane proteins that have previously been associated with sensory functions. These include several ion channels (*Grid2*, *Trpa1*, *Gabrg1, Chrna3*, *Htr3b*, *Ano1*) and other functional transmembrane receptors (*Gpr65*, *Tmem233*) thought to be involved in visceral and/or somatotopic sensory signaling (Dietrich et al., 2022; Jami et al., 2023; Kashio & Tominaga, 2022; Khan et al., 2023; H. Kim et al., 2024; Morales & Wang, 2002; Prato et al., 2017; Sisignano et al., 2021). While each cluster differentially expressed a unique combination of transcripts, we found that most genes were expressed in multiple clusters. Moreover, gene expression patterns generally supported the phenotypic clustering of chemosensory and mechanosensory neuronal types, though many genes were nonetheless found to be expressed in both classes of neurons. Chemosensory *Scn10a*+ clusters, for example, preferentially expressed *Gpr65*, *Htr3b*, *Esr1*, and *Trpa1*. By contrast, mechanosensory *Scn10a*+ clusters preferentially expressed *Grid2*, *Galnt18*, and *Tmem233*. Mechanosensory *Scn1a*+ clusters typically expressed *Ankrd24*, *Egfem1*, *Tafa2*, and *Atp2b2*, with some subtypes defined by the additional expression of specific surface receptors including *Ntrk3*, *Gabrg1*, or *Ano1*. Some NG clusters expressed low levels of both *Scn1a* and *Scn10a,* and these clusters displayed more distinct gene expression profiles. Among these are 2 clusters with high expression of *Apoe* and *Sparc*, which may indicate stressed or injured neurons, or the inclusion of glial cells in our analyses despite our filtering procedures (Boyles et al., 1985; Gillen et al., 1995; Vincent et al., 2008; Xu et al., 2006). Other clusters in this group were defined by expression of the nicotinic acetylcholine receptor subunit *Chrna3*, and/or several genes associated with axonal or dendritic migration and

pruning, including *Chn2*, *St18*, and *Xylt1*, suggestive of a particularly high degree of morphological plasticity in these NG neuron types.

We further examined the expression of several genes previously identified in the literature to be strongly expressed in NG neurons innervating the heart (Wang et al., 2009), lungs (Brouns et al., 2000; S. H. Kim et al., 2022; Lee et al., 2015), and/or gut (Dockray & Burdyga, 2011; Egerod et al., 2018; Yu et al., 2016) (**Figure 2B**). We note that many of these are also included among the cluster-defining genes shown in **Figure 2A**, supporting the validity of our computational approach to clustering NG neurons. In this targeted subset of genes, we again find that the majority are expressed in multiple putative mechanosensing and chemosensing clusters, though expression tends to support hierarchical clustering of our subtypes along these functional lines. Consistent with published literature, we find that expression of *Oprm1* (mu-1 opioid receptor), *P2rx3* (P2X purinergic receptor 3), and *Cnr1* (endocannabinoid receptor 1) are particularly ubiquitously expressed across almost all NG clusters (Burdyga et al., 2010; Búzás & Cox, 1997; Xiang et al., 1998).

Overall, we find a high degree of overlapping gene expression across NG clusters in rats, though all clusters can be defined by unique combinatorial expression of several genes.

Weak differential right-left gene expression within NG clusters

To begin to examine the possible genetic basis of lateralized vagal reward signaling, we performed a pseudobulk analysis of differential gene expression within each of our 22 clusters (Zimmerman et al., 2021). This analysis revealed only three

clusters in which any genes were found to be significantly differentially expressed. In the UMAP visualization and hierarchical clustering tree, these clusters were situated near each other, suggesting a degree of similarity in their genetic profiles. Across all three clusters, 10 significantly differentially expressed genes were identified (**Figure 3A**). Expression of two of these genes, *Opcml* (opioid binding protein/cell adhesion molecule) and *Gria1* (AMPA receptor subunit 1), were found to be significantly left-NG biased in multiple clusters. Overall, however, even when differential gene expression was observed within a cluster, the effect sizes and significance levels were small (**Figure 3C**). These findings suggest that in naïve rats, cell-type specific expression of differential sensory receptors may not be a major driver of lateralized vagal reward signaling.

A *Chrna3* and *Cckar* expressing cluster is preferentially found in right nodose ganglia

To test whether the identified cell types themselves might be differentially expressed between right and left NG, we analyzed cell counts from each cluster to determine if that cluster contained a greater-than-expected number of cells on the left or right side. Across the entire dataset, we observed that the percentage of cells from right NG was slightly higher than the percentage of cells from left NG (56% vs. 44%, respectively). For each individual cluster, we thus compared the percentage of cells from the right or left NG to this expected distribution using multiple Bonferroni-corrected binomial tests. This statistical analysis revealed two clusters with significantly lateralized expression (**Figure 3C**). Cluster #5 comprised ca. 7% of the overall NG population and

was significantly biased toward right-side expression. This cluster was defined by high levels of expression of *Chrna3, Xylt1,* and *Cckar*. Cluster #6 comprised ca. 6% of the overall dataset, was significantly biased toward left-side expression, and was defined by expression of *Cysltr2*, *Gdpd4*, and *Trpc3*.

Cholecystokinin A receptors (CCKARs) are strongly expressed in gut-innervating NG neurons and are known to regulate satiety and macronutrient sensing (Cawthon & de La Serre, 2021; Dockray, 2009; Rogers & Hermann, 2008; Smith et al., 1981). CCK has also been shown to play a role in the vagal signaling pathways that shape nutrient preferences (Buchanan et al., 2022; Li et al., 2022; McDougle et al., 2024). Right-biased expression of a *Cckar*-expressing cluster of NG neurons thus provides a strong candidate for driving lateralized vagal reward-related signaling. To validate right-biased expression of *Cckar*-expressing NG neurons, we used RNA fluorescence in situ hybridization (RNA-FISH) to quantify *Chrna3*+, *Cckar*+, and co-labeled cells in left versus right NG from six rats. Our results confirmed overlapping expression of *Chrna3* and *Cckar* in the majority of *Cckar*+ NG neurons, though we also found that many cells express *Chrna* without co-expressing *Cckar*. Consistent with our computational results, *Cckar*+ neurons were found to be significantly more numerous in right NG compared to left (Percent *Cckar*+: Left: 11.8 ± 0.90%, Right: 19.6 ± 1.82%; $p = 0.0158$, paired t-test), though the average number of NG neurons did not differ (Average *Snap25*+ per slice across rats: Left: 223.04 ± 22.78, Right: 254.61 ± 21.04; $p = 0.4230$, paired t-test). Interestingly, no significant difference was found between right and left NG expression of *Chrna3*+ neurons (Left: 19.97 ± 2.28% , Right: 24.77 ± 2.51%; $p = 0.07$, paired t-test),

further implicating *Cckar*+ neurons in the asymmetric encoding of interoceptive rewards (**Figures 3D-E**).

Using a publicly available dataset (GEO #GSE185173) (Buchanan et al., 2022), we further validated right-side bias of a *Cckar*-expressing NG cluster in mice. The mouse and rat datasets were integrated and re-clustered, applying the same computational protocols as before. This analysis resulted in the identification of 21 clusters in the integrated dataset (**Figure 4A**), with strong overlap between the mouse and rat data (**Figures 4B-C**). We repeated the analysis of cell counts using the integrated dataset to determine whether any clusters exhibited significant preferential expression in the right or left NG. This statistical analysis identified two clusters with significantly lateralized expression (**Figure 3C**). One of these clusters (#11) was strongly dominated by the mouse dataset and expressed relatively high levels of *Apoe* and *Sparc*, again suggestive of an injured or non-neuronal phenotype. The other (Cluster #6) represented the same cluster previously identified as right-side biased in the rat-only dataset, defined by high levels of expression of *Chrna3, Xylt1,* and *Cckar*. In both mice and rats, this cluster was well-represented, making up 7-8% of the total sample. Interestingly, while several marker genes defined this cluster in both the rat and mouse datasets, many other well-known NG genes associated with gut-brain signaling were found to be much more strongly co-expressed in this cluster in mice compared to rats (e.g., *Cartpt*, *Npy2r*, *Vip*), highlighting the differential genetic complexity of NG neurons across the two species. Nonetheless, combined, our results strongly suggest that *Cckar*-expressing neurons are preferentially expressed in the right NG over the left in both mice and rats. These findings are consistent with a lateralized vagal reward

pathway that likely arises from gut-innervating fibers and point to CCKARs in particular as a possible mediator of this lateralized reward signaling.

DISCUSSION

Our data represent the first scRNA-seq analysis of NG neurons in rats, providing an important resource to the neuroscientific community. In the current study, we aimed to utilize this dataset to determine whether genetic differences in right vs. left NG neurons contribute to asymmetric encoding of visceral reward-related signaling by the vagus nerve. Our analyses identified a cluster of *Cckar*+ and *Chrna3*+ neurons that are preferentially expressed in the right NG of both rats and mice, implicating these gut-innervating nutrient sensors in the lateralized encoding of interoceptive rewards.

Our clustering results in rats are largely consistent with prior work in mice that has demonstrated distinct mechanosensing vs. chemosensing NG subtypes (Bai et al., 2019; Kupari et al., 2019; Zhao et al., 2022). As in mice, we find that chemosensory neurons represent the majority of NG clusters and preferentially express *Scn10a* and *Oprm1*. Following Kupari et al. (2019), we have tentatively labeled such cells "nociceptor-like", reflecting broad similarly with well-characterized nociceptive neurons in dorsal root ganglia of the spinal cord. However, the extent to which these NG clusters perform nociceptive functions remains unknown.

Mechanosensitive *Piezo2*+ clusters represent a smaller proportion of NG neurons and most of these clusters express *Scn1a* over *Scn10a*. Our analyses identified 22 NG clusters in rats, which is slightly more than the 18 NG clusters identified by Kupari et al. in mice. This likely reflects both a true enhanced genetic diversity in the larger rodent species, as well as minor differences in sequencing and computational clustering approaches. Notably, we were able to putatively match our clusters to those of Kupari et al. based on expression of several key genes, and our integrated analysis of rat and

mouse samples provides further support for a broadly similar NG gene expression across the two species.

While we find substantive similarities in NG gene expression between rats and mice, important differences are also evident between the two species. In our rat dataset, we found no evidence of a dopamine beta hydroxylase-expressing (DBH+) NG cluster, though several studies have reported such cells in mice (Buchanan et al., 2022; Kupari et al., 2019). The presence of DBH+ neurons in mouse NG datasets may reflect the difficulty of isolating the vagal ganglia in the smaller species, which can fuse with glossopharyngeal and/or superior cervical ganglia in rodents (Altschuler et al., 1989; Bookout & Gautron, 2021). We also find that the chemosensing clusters associated with weak differential within-cluster gene expression were not found in mice, which may support expanded genetic diversity among NG cell types in rats. We further observed that *Apoe*+ cell types were largely non-overlapping in mice and rats, which may reflect species-specificity of non-neuronal cell types in the NG, or differences in NG neuronal responses to injury between the two species.

Overall, we find a high degree of overlapping gene expression across NG clusters in rats, though all clusters can be defined by unique combinatorial expression of several genes. Interestingly, we find that several genes that are associated with digestive signaling, including leptin receptors (*Lepr*), glucagon-like peptide-1 receptors (*Glp1r*), and cocaine and amphetamine regulated transcript (*Cartpt*), exhibited weak and largely non-overlapping expression across multiple clusters in our rat data. These results suggest to us that the majority of our computationally identified clusters may represent subpopulations of NG neurons that project to multiple organ systems, which is

consistent with the massively branching anatomy of the vagus nerve but complicates efforts to genetically target organ-specific visceral signaling pathways in the rat.

Our results demonstrate that there is right-biased expression of a *Cckar*+ and *Chrna3*+ subtype of NG neuron in rats and mice. Cholecystokinin (CCK) is a peptide released by enteroendocrine cells in the gastrointestinal tract in response to food intake, and CCKARs are strongly expressed in gut-innervating NG neurons (Cawthon & de La Serre, 2021; Dockray, 2009; Rogers & Hermann, 2008). CCKARs play an important role in regulating satiety and sensing macronutrients through gut-brain vagal signaling pathways. CCK has also been found to play a critical role in shaping the preference for macronutrients including fat, sugar, and amino acids (Buchanan et al., 2022; Li et al., 2022; McDougle et al., 2024). Right-biased expression of *Cckar*+ NG neurons thus provides a strong candidate for mediating lateralized vagal reward-related signaling in future studies.

MATERIALS AND METHODS

All procedures were conducted in accordance with the National Institutes of Health Guide for the Care and Use of Laboratory Animals and were approved by the University of Texas Institutional Animal Care and Use Committee.

Experimental design: The right and left NG of experimentally naïve, 8-week-old male (n=18) and female (n=18) rats were dissected, and single-cell RNA sequencing (scRNA-Seq) was performed. scRNA-seq was performed on NG samples from 12 replicate groups (3 Male|Left, 3 Male|Right, 3 Female|Left, 3 Female|Right); each replicate group was created by pooling left or right NG samples from six rats (**Figure 1A**). Samples were prepared using a Parse Biosciences Evercode Nuclei Fixation Kit v2 (ECF2003) and Parse Single Cell Whole Transcriptome Kit v2 (ECW02130) and sequenced on an Illumina Nextseq 2000 at the Genome Center at the University of Texas at Dallas. Clustering and statistical analyses were performed in R version 4.3.2 (R Core Team, 2023)using Seurat v4.1.3 (Hao et al., 2021). Computational results were validated using RNA fluorescence in situ hybridization (RNA-FISH) to quantify expression of key transcripts in NG samples collected from an additional 6 rats (3 male, 3 female).

Nodose ganglia sample collection: For scRNA-seq samples, rats were deeply anesthetized with 5% isoflurane and sacrificed via rapid decapitation. The right and left NG were dissected and stored in separate PCR tubes before flash-freezing on dry ice. The first side of dissection was counterbalanced across rats. NG samples were stored in a -80 ºC freezer until sample preparation.

For RNA-FISH samples, rats were deeply anesthetized with sodium pentobarbital and transcardially perfused with cold phosphate buffered saline (PBS) followed by 4% paraformaldehyde (PFA) in PBS. NG were dissected, embedded in OCT, quickly frozen over dry ice and stored at -80 ºC until sectioning. Slices were made at 20 µm thickness using a Leica CN1860 Cryostat and directly mounted on slides. Slides were stored at -80 ºC until RNA-FISH was performed.

Sample Preparation and Sequencing: Individual NG were pooled to prepare three replicate groups for each of the four treatment groups (Male|Left; Male|Right; Female|Left; Female|Right). Each replicate group was created by pooling the right or left NG samples from 6 rats (**Figure 1A**). Nuclei were fixed and barcoded according to Parse Biosciences protocols (Evercode Version 2 Nuclei Fixation Kit, Version 2 WT Kit). The samples were split into 8 sublibraries and were sequenced via paired-end sequencing using the Illumina Nextseq 2000 at the Genome Center at the University of Texas at Dallas.

scRNA-Seq Analysis: Data was preprocessed using the Parse Biosciences Cloud-Based Pipeline to obtain cell-gene count matrices for each replicate group. Sequencing data was then analyzed with R (version 4.3.2) using Seurat (version 4.1.3). The 12 replicate groups generated a total of 36741 sequenced cells with an average of ca. 32,000 reads/cell and ca. 1500 genes detected per cell. Cells were filtered using quality control metrics (500-6,500 genes per cell, mitochondrial genes < 1.5%), removing 139 poor-quality cells. Additional filtering was performed to remove cells expressing high levels of marker genes for muscle (*Ttn*, *Myh4*), myelin (*Mbp*, *Mpz*), and jugular neurons (*Prdm12*), and to restrict

our analysis to cells expressing high levels of the neuronal marker *Snap25*, resulting in a dataset of putative NG-specific neurons comprised of 9879 cells. Data from each treatment group was integrated, scaled, and clustered using default parameters in Seurat.

Cluster-specific marker genes were identified using Wilcoxon rank-sum tests with Bonferroni corrections. To test for differential gene expression between right and left samples, pseudobulk analysis was used (Zimmerman et al., 2021). For each cluster, data from all replicate groups was aggregated and differential right vs. left gene expression was calculated using Bonferroni-corrected Wilcoxon rank-sum tests. To test for lateralized cell counts for each identified cluster, we used Bonferroni-corrected binomial tests. For each cluster identified as having significant left or right-side biased counts, we performed additional binomial tests to validate that this bias was observed in both male and female samples. Statistical results are reported as significant for corrected $p < 0.05$.

To compare the lateralized expression of NG clusters in rats and mice, we integrated our rat scRNA-seq data with a publicly available mouse NG sequencing dataset of 5,507 cells in which right and left samples were similarly separately identified (Buchanan et al., 2022). The integrated rat + mouse dataset was filtered using quality control metric thresholds based on the feature distributions found in the mouse dataset (1000-7500 genes per cell, mitochondrial genes < 5%). The integrated dataset was further filtered to restrict analysis to putative NG neurons as described above, resulting in an integrated dataset comprised of 9,198 cells (mouse: n = 1,081; rat: n = 8,117). Data was then scaled and clustered using default parameters in Seurat. We tested for lateralized cell counts for each identified cluster separately in rats and mice using Bonferroni-corrected binomial tests. Statistical significance is reported for corrected $p < 0.05$.

In situ hybridization: Hybridization chain reaction RNA fluorescence *in situ* hybridization (HCR RNA-FISH v3.0; Molecular Instruments) was used to validate differential right vs. left NG expression of the computationally identified right-biased *Chrna3*+ and *Cckar*+ cluster. Hybridization probes sets targeting *Chrna3, Cckar*, and *Snap25* were custom designed based on the transcript sequences found in NCBI (NCBI Accession numbers: *Snap25:* NM_030991, *Cckar:* NM_012688, *Chrna3:* NM_052805). Multiplexed staining was performed using an HCR RNA-FISH kit including the three probe sets, probe channel specific HCR amplifiers (each consisting of a pair of fluorophore-tethered hairpins), as well as hybridization, wash, and amplification buffers.

HCR™ RNA-FISH was performed according to adapted vendor protocols (Choi et al., 2018). After removing samples from -80°C, slides were immediately immersed at room temperature in 100% ethanol for 15 minutes, followed by immersion in 100% ethanol for 5 minutes, then immersed once in 1X PBS briefly to wash off remaining OCT. Slides were then air dried and a hydrophobic barrier was drawn around the tissue using the ImmEdge® Hydrophobic Barrier PAP pen (H-4000, Vector Laboratories). Probe hybridization buffer was carefully added on top of the samples and allowed to pre-hybridize for 10 minutes in a humidified chamber using HybEZ II oven (#240200, ACD) at 37 °C. A probe solution was prepared by adding 2.5 µL of each *Snap25*, *Chrna3*, and *Cckar* hybridization probe set (1 µM stock) in 100 µL of pre-heated probe hybridization buffer solution at 37 °C. If needed, more probe solution was prepared at the same ratio of probe set and hybridization buffer as described. Any pre-hybridization solution was removed from slides by flicking the slides before the probe solution was added on top of the samples and

incubated overnight (> 20 hrs) at 37 °C. As a negative control, one slide was treated with hybridization solution with no gene probes so there would be no initiator to trigger growth of the fluorescent amplification polymer.

The following day, slides were washed in a series of mixed and pre-heated probe wash buffer and 5X Saline Sodium Citrate buffer (SSCT) (BP1325, Fisher) solutions at 37 °C for 15 min each in the following order: (1) 75% probe wash buffer with 25% 5X SSCT, (2) 50% probe wash buffer with 50% 5X SSCT, (3) 25% probe wash buffer with 75% 5X SSCT, and (4) 100% 5X SSCT. This was followed by a 5 min wash in 100% 5X SSCT at room temperature. Amplification buffer was added on top of the samples, and slides were pre-amplified in the humidified chamber for 30 minutes at room temperature. Hairpin dyes were snap-cooled by incubating at 95°C for 90 seconds then immediately cooled at room temperature in the dark for at least 30 minutes. The snap-cooled hairpins were added to the amplification buffer to create a hairpin solution. The pre-amplification buffer was removed from the slides and the hairpin solution was added on top of the samples and incubated overnight in a humidified chamber at room temperature.

The next day, slides were washed in 100% 5X SSCT twice for 30 min and then once for 5 min. An autofluorescence quenching solution was created by making a 1:1:1 solution of reagents in the Vector® TrueVIEW® Autofluorescence Quenching Kit (SP-8400-15, Vector Laboratories). This solution was added on top of the samples and incubated for 3.5 minutes, then slides were washed in 1X PBS for 5 minutes at room temperature. Slides were cover slipped with VectaShield® Vibrance® Antifade Mounting Medium with DAPI (H-1800-10, Vector Laboratories) and sealed with nail polish. Slides were imaged within 24 hours.

FISH imaging and image analysis: An Olympus FV3000RS confocal microscope was used to capture images. The same acquisition parameters were used for all experimental samples and negative controls. Two to six slices per ganglia were imaged at 20X for semi-automated cell counting. Multiple images with overlapping fields of view were taken to capture the entirety of each slice, and images were stitched together to reconstruct whole-slice images in each channel (Preibisch et al., 2009). Image analysis was performed using FIJI (Schindelin et al., 2012). Image quantification was performed by a blinded experimenter. Stitched images were smoothed using a 3x3 mean filter, then thresholded using channel-specific pixel intensity cutoffs based on signal-to-noise ratios (*Snap25*: 500-Maximum, *Chrna3*: 900-Maximum, *Cckar*: 1200-Maximum; 16 bit images) Cells were then automatically detected using particle analysis for particles larger than 50 pixels. This process generated image masks comprised of detected cells, from which cell counts for each individual channel (*Chrna3*, *Cckar*, and *Snap25*) were obtained. For each slice, *Cckar*+/*Chrna3*+ co-expression was manually quantified by a blinded experimenter using overlaid *Chrna3* and *Cckar* channel masks. The number of *Snap25*+ neurons per slice was counted and averaged for each animal. The percentages of *Cckar*+, *Chrna3*+, and *Cckar*+/*Chrna3*+ colabeled neurons were then calculated for each slice, and these percentages were averaged across slices for each animal. Paired t-tests were used to test for lateralized expression of *Snap25*+, *Cckar*+, *Chrna3*+, or *Cckar*+/*Chrna3*+ colabeled neurons. Statistical significance is reported for $p < 0.05$.

Data Availability

Raw and processed single-cell sequencing data are available on the Gene Expression Omnibus (GEO) under accession number GSE280062.

Acknowledgements

This work was funded by NIH R21 DA055166, R01 NS126816, R01 NS065926, R01 DK115478, and F31 NS129269. We thank Dr. Adriana Shembel, Dr. Robert Morrison, and Dr. I-Fan Mau for their technical assistance in establishing NG dissection protocols.

Author contributions

HFW participated in conceptualization, investigation, formal analysis, visualization, data curation, and writing – original draft; VMH, IS, and KM participated in investigation and writing – review & editing; BJK and TJP participated in supervision, writing – review & editing, and funding acquisition; CAT participated in conceptualization, formal analysis, data curation, writing – original draft, project administration, and funding acquisition.

Declaration of Interests

The authors declare no competing interests.

References

Altschuler, S. M., Bao, X., Bieger, D., Hopkins, D. A., & Miselis, R. R. (1989). Viscerotopic representation of the upper alimentary tract in the rat: Sensory ganglia and nuclei of the solitary and spinal trigeminal tracts. *Journal of Comparative Neurology*, *283*(2). https://doi.org/10.1002/cne.902830207

Ardell, J. L., & Randall, W. C. (1986). Selective vagal innervation of sinoatrial and atrioventricular nodes in canine heart. *American Journal of Physiology - Heart and Circulatory Physiology*. https://doi.org/10.1152/ajpheart.1986.251.4.h764

Bai, L., Mesgarzadeh, S., Ramesh, K. S., Huey, E. L., Liu, Y., Gray, L. A., Aitken, T. J., Chen, Y., Beutler, L. R., Ahn, J. S., Madisen, L., Zeng, H., Krasnow, M. A., & Knight, Z. A. (2019). Genetic Identification of Vagal Sensory Neurons That Control Feeding. *Cell*, *179*(5). https://doi.org/10.1016/j.cell.2019.10.031

Berthoud, H. R., Albaugh, V. L., & Neuhuber, W. L. (2021). Gut-brain communication and obesity: Understanding functions of the vagus nerve. In *Journal of Clinical Investigation*. https://doi.org/10.1172/JCI143770

Berthoud, H. R., & Neuhuber, W. L. (2000). Functional and chemical anatomy of the afferent vagal system. *Autonomic Neuroscience: Basic and Clinical*. https://doi.org/10.1016/S1566-0702(00)00215-0

Bookout, A. L., & Gautron, L. (2021). Characterization of a cell bridge variant connecting the nodose and superior cervical ganglia in the mouse: Prevalence, anatomical features, and practical implications. *Journal of Comparative Neurology*, *529*(1). https://doi.org/10.1002/cne.24936

Boyles, J. K., Pitas, R. E., Wilson, E., Mahley, R. W., & Taylor, J. M. (1985). Apolipoprotein E associated with astrocytic glia of the central nervous system and with nonmyelinating glia of the peripheral nervous system. *Journal of Clinical Investigation*, *76*(4). https://doi.org/10.1172/JCI112130

Brougher, J., Aziz, U., Adari, N., Chaturvedi, M., Jules, A., Shah, I., Syed, S., & Thorn, C. A. (2021). Self-Administration of Right Vagus Nerve Stimulation Activates Midbrain Dopaminergic Nuclei. *Frontiers in Neuroscience*, *15*, 782786. https://doi.org/10.3389/fnins.2021.782786

Brouns, I., Adriaensen, D., Burnstock, G., & Timmermans, J. P. (2000). Intraepithelial vagal sensory nerve terminals in rat pulmonary neuroepithelial bodies express P2X3 receptors. *American Journal of Respiratory Cell and Molecular Biology*, *23*(1). https://doi.org/10.1165/ajrcmb.23.1.3936

Buchanan, K. L., Rupprecht, L. E., Kaelberer, M. M., Sahasrabudhe, A., Klein, M. E., Villalobos, J. A., Liu, W. W., Yang, A., Gelman, J., Park, S., Anikeeva, P., & Bohórquez, D. V. (2022). The preference for sugar over sweetener depends on a gut sensor cell. *Nature Neuroscience*, *25*(2). https://doi.org/10.1038/s41593-021-00982-7

Burdyga, G., Varro, A., Dimaline, R., Thompson, D. G., & Dockray, G. J. (2010). Expression of cannabinoid CB1 receptors by vagal afferent neurons: Kinetics and role in influencing neurochemical phenotype. *American Journal of Physiology - Gastrointestinal and Liver Physiology*, *299*(1). https://doi.org/10.1152/ajpgi.00059.2010

Búzás, B., & Cox, B. M. (1997). Quantitative analysis of Mu and delta opioid receptor gene expression in rt brain and peripheral ganglia using competitive polymerase chain reaction. *Neuroscience*, *76*(2). https://doi.org/10.1016/S0306-4522(96)00242-4

Capilupi, M. J., Kerath, S. M., & Becker, L. B. (2020). Vagus nerve stimulation and the cardiovascular system. *Cold Spring Harbor Perspectives in Medicine*, *10*(2). https://doi.org/10.1101/cshperspect.a034173

Cawthon, C. R., & de La Serre, C. B. (2021). The critical role of CCK in the regulation of food intake and diet-induced obesity. *Peptides*, *138*. https://doi.org/10.1016/j.peptides.2020.170492

Choi, H. M. T., Schwarzkopf, M., Fornace, M. E., Acharya, A., Artavanis, G., Stegmaier, J., Cunha, A., & Pierce, N. A. (2018). Third-generation in situ hybridization chain reaction: Multiplexed, quantitative, sensitive, versatile, robust. *Development (Cambridge)*, *145*(12). https://doi.org/10.1242/dev.165753

Dietrich, S., Company, C., Song, K., Lowenstein, E. D., Riedel, L., Birchmeier, C., Gargiulo, G., & Zampieri, N. (2022). Molecular identity of proprioceptor subtypes innervating different muscle groups in mice. *Nature Communications*, *13*(1). https://doi.org/10.1038/s41467-022-34589-8

Dockray, G. J. (2009). Cholecystokinin and gut-brain signalling. In *Regulatory Peptides* (Vol. 155, Issues 1–3). https://doi.org/10.1016/j.regpep.2009.03.015

Dockray, G. J., & Burdyga, G. (2011). Plasticity in vagal afferent neurones during feeding and fasting: Mechanisms and significance. In *Acta Physiologica* (Vol. 201, Issue 3). https://doi.org/10.1111/j.1748-1716.2010.02219.x

Egerod, K. L., Petersen, N., Timshel, P. N., Rekling, J. C., Wang, Y., Liu, Q., Schwartz, T. W., & Gautron, L. (2018). Profiling of G protein-coupled receptors in vagal afferents reveals novel gut-to-brain sensing mechanisms. *Molecular Metabolism*, *12*. https://doi.org/10.1016/j.molmet.2018.03.016

Gillen, C., Gleichmann, M., Spreyer, P., & Müller, H. W. (1995). Differentially expressed genes after peripheral nerve injury. *Journal of Neuroscience Research*, *42*(2). https://doi.org/10.1002/jnr.490420203

Han, W., Tellez, L. A., Perkins, M. H., Perez, I. O., Qu, T., Ferreira, J., Ferreira, T. L., Quinn, D., Liu, Z. W., Gao, X. B., Kaelberer, M. M., Bohórquez, D. V., Shammah-Lagnado, S. J., de Lartigue, G., & de Araujo, I. E. (2018). A Neural Circuit for Gut-Induced Reward. *Cell*. https://doi.org/10.1016/j.cell.2018.08.049

Hao, Y., Hao, S., Andersen-Nissen, E., Mauck, W. M., Zheng, S., Butler, A., Lee, M. J., Wilk, A. J., Darby, C., Zager, M., Hoffman, P., Stoeckius, M., Papalexi, E., Mimitou, E. P., Jain, J., Srivastava, A., Stuart, T., Fleming, L. M., Yeung, B., … Satija, R. (2021). Integrated analysis of multimodal single-cell data. *Cell*, *184*(13). https://doi.org/10.1016/j.cell.2021.04.048

Jami, S., Deuis, J. R., Klasfauseweh, T., Cheng, X., Kurdyukov, S., Chung, F., Okorokov, A. L., Li, S., Zhang, J., Cristofori-Armstrong, B., Israel, M. R., Ju, R. J., Robinson, S. D., Zhao, P., Ragnarsson, L., Andersson, Å., Tran, P., Schendel, V., McMahon, K. L., … Vetter, I. (2023). Pain-causing stinging nettle toxins target TMEM233 to modulate NaV1.7 function. *Nature Communications*, *14*(1). https://doi.org/10.1038/s41467-023-37963-2

Kashio, M., & Tominaga, M. (2022). TRP channels in thermosensation. In *Current Opinion in Neurobiology* (Vol. 75). https://doi.org/10.1016/j.conb.2022.102591

Khan, Z., Jung, M., Crow, M., Mohindra, R., Maiya, V., Kaminker, J. S., Hackos, D. H., Chandler, G. S., McCarthy, M. I., & Bhangale, T. (2023). Whole genome sequencing across clinical trials identifies rare coding variants in GPR68 associated with chemotherapy-induced peripheral neuropathy. *Genome Medicine*, *15*(1). https://doi.org/10.1186/s13073-023-01193-4

Kim, H., Shim, W.-S., & Oh, U. (2024). Anoctamin 1, a multi-modal player in pain and itch. *Cell Calcium*, *123*, 102924. https://doi.org/10.1016/j.ceca.2024.102924

Kim, S. H., Patil, M. J., Hadley, S. H., Bahia, P. K., Butler, S. G., Madaram, M., & Taylor-Clark, T. E. (2022). Mapping of the Sensory Innervation of the Mouse Lung by Specific Vagal and Dorsal Root Ganglion Neuronal Subsets. *ENeuro*, *9*(2). https://doi.org/10.1523/ENEURO.0026-22.2022

Kupari, J., Häring, M., Agirre, E., Castelo-Branco, G., & Ernfors, P. (2019). An Atlas of Vagal Sensory Neurons and Their Molecular Specialization. *Cell Reports*, *27*(8). https://doi.org/10.1016/j.celrep.2019.04.096

Lee, L. Y., Hsu, C. C., Lin, Y. J., Lin, R. L., & Khosravi, M. (2015). Interaction between TRPA1 and TRPV1: Synergy on pulmonary sensory nerves. *Pulmonary Pharmacology and Therapeutics*, *35*. https://doi.org/10.1016/j.pupt.2015.08.003

Li, M., Tan, H. E., Lu, Z., Tsang, K. S., Chung, A. J., & Zuker, C. S. (2022). Gut–brain circuits for fat preference. *Nature*, *610*(7933). https://doi.org/10.1038/s41586-022-05266-z

Maniscalco, J. W., & Rinaman, L. (2018). Vagal interoceptive modulation of motivated behavior. In *Physiology* (Vol. 33, Issue 2). https://doi.org/10.1152/physiol.00036.2017

Mazzone, S. B., & Undem, B. J. (2016). Vagal afferent innervation of the airways in health and disease. *Physiological Reviews*, *96*(3). https://doi.org/10.1152/physrev.00039.2015

McDougle, M., de Araujo, A., Singh, A., Yang, M., Braga, I., Paille, V., Mendez-Hernandez, R., Vergara, M., Woodie, L. N., Gour, A., Sharma, A., Urs, N., Warren, B., & de Lartigue, G. (2024). Separate gut-brain circuits for fat and sugar reinforcement combine to promote overeating. *Cell Metabolism*, *36*(2). https://doi.org/10.1016/j.cmet.2023.12.014

Morales, M., & Wang, S. De. (2002). Differential composition of 5-hydroxytryptamine3 receptors synthesized in the rat CNS and peripheral nervous system. *Journal of Neuroscience*, *22*(15). https://doi.org/10.1523/jneurosci.22-15-06732.2002

Prato, V., Taberner, F. J., Hockley, J. R. F., Callejo, G., Arcourt, A., Tazir, B., Hammer, L., Schad, P., Heppenstall, P. A., Smith, E. S., & Lechner, S. G. (2017). Functional and Molecular Characterization of Mechanoinsensitive “Silent” Nociceptors. *Cell Reports*, *21*(11). https://doi.org/10.1016/j.celrep.2017.11.066

Preibisch, S., Saalfeld, S., & Tomancak, P. (2009). Globally optimal stitching of tiled 3D microscopic image acquisitions. *Bioinformatics*, *25*(11). https://doi.org/10.1093/bioinformatics/btp184

Prescott, S. L., & Liberles, S. D. (2022). Internal senses of the vagus nerve. In *Neuron* (Vol. 110, Issue 4). https://doi.org/10.1016/j.neuron.2021.12.020

Prescott, S. L., Umans, B. D., Williams, E. K., Brust, R. D., & Liberles, S. D. (2020). An Airway Protection Program Revealed by Sweeping Genetic Control of Vagal Afferents. *Cell*, *181*(3). https://doi.org/10.1016/j.cell.2020.03.004

R Core Team. (2023). R: A language and environment for statistical computing. In *Computing* (4.3.2; Vol. 20). R Foundation for Statistical Computing. https://www.R-project.org

Rogers, R. C., & Hermann, G. E. (2008). Mechanisms of action of CCK to activate central vagal afferent terminals. *Peptides*, *29*(10). https://doi.org/10.1016/j.peptides.2008.06.023

Schindelin, J., Arganda-Carreras, I., Frise, E., Kaynig, V., Longair, M., Pietzsch, T., Preibisch, S., Rueden, C., Saalfeld, S., Schmid, B., Tinevez, J. Y., White, D. J., Hartenstein, V., Eliceiri, K., Tomancak, P., & Cardona, A. (2012). Fiji: An open-source platform for biological-image analysis. In *Nature Methods* (Vol. 9, Issue 7). https://doi.org/10.1038/nmeth.2019

Schwartz, G. J. (2000). The role of gastrointestinal vagal afferents in the control of food intake: Current prospects. *Nutrition*. https://doi.org/10.1016/S0899-9007(00)00464-0

Sisignano, M., Fischer, M. J. M., & Geisslinger, G. (2021). Proton-sensing gpcrs in health and disease. In *Cells* (Vol. 10, Issue 8). https://doi.org/10.3390/cells10082050

Sitdikov, F. G., Gil'mutdinova, R. I., Minnakhmetov, R. R., & Zefirov, T. L. (2000). Asymmetrical effects of vagus nerves on functional parameters of rat heart in

postnatal ontogeny. *Bulletin of Experimental Biology and Medicine*, *130*(1). https://doi.org/10.1007/bf02682086

Smith, G. P., Jerome, C., Cushin, B. J., Eterno, R., & Simansky, K. J. (1981). Abdominal vagotomy blocks the satiety effect of cholecystokinin in the rat. *Science*, *213*(4511). https://doi.org/10.1126/science.7268408

Stuart, T., Butler, A., Hoffman, P., Hafemeister, C., Papalexi, E., Mauck, W. M., Hao, Y., Stoeckius, M., Smibert, P., & Satija, R. (2019). Comprehensive Integration of Single-Cell Data. *Cell*, *177*(7). https://doi.org/10.1016/j.cell.2019.05.031

Teckentrup, V., & Kroemer, N. B. (2024). Mechanisms for survival: vagal control of goal-directed behavior. In *Trends in Cognitive Sciences* (Vol. 28, Issue 3). https://doi.org/10.1016/j.tics.2023.11.001

Vincent, A. J., Lau, P. W., & Roskams, A. J. (2008). SPARC is expressed by macroglia and microglia in the developing and mature nervous system. *Developmental Dynamics*, *237*(5). https://doi.org/10.1002/dvdy.21495

Wang, Y., Li, G., Yu, K., Liang, S., Wan, F., Xu, C., Gao, Y., Liu, S., & Lin, J. (2009). Expressions of P2X2 and P2X3 receptors in rat nodose neurons after myocardial ischemia injury. *Autonomic Neuroscience: Basic and Clinical*, *145*(1–2). https://doi.org/10.1016/j.autneu.2008.11.006

Woodbury, D. M., & Woodbury, J. W. (1990). Effects of Vagal Stimulation on Experimentally Induced Seizures in Rats. *Epilepsia*, *31*. https://doi.org/10.1111/j.1528-1157.1990.tb05852.x

Xiang, Z., Bo, X., & Burnstock, G. (1998). Localization of ATP-gated P2X receptor immunoreactivity in rat sensory and sympathetic ganglia. *Neuroscience Letters*, *256*(2). https://doi.org/10.1016/S0304-3940(98)00774-5

Xu, Q., Bernardo, A., Walker, D., Kanegawa, T., Mahley, R. W., & Huang, Y. (2006). Profile and regulation of apolipoprotein E (ApoE) expression in the CNS in mice with targeting of green fluorescent protein gene to the ApoE locus. *Journal of Neuroscience*, *26*(19). https://doi.org/10.1523/JNEUROSCI.5476-05.2006

Yamakawa, K., So, E. L., Rajendran, P. S., Hoang, J. D., Makkar, N., Mahajan, A., Shivkumar, K., & Vaseghi, M. (2014). Electrophysiological effects of right and left vagal nerve stimulation on the ventricular myocardium. *American Journal of Physiology - Heart and Circulatory Physiology*, *307*(5). https://doi.org/10.1152/ajpheart.00279.2014

Yu, X., Yu, M., Liu, Y., & Yu, S. (2016). TRP channel functions in the gastrointestinal tract. In *Seminars in Immunopathology* (Vol. 38, Issue 3). https://doi.org/10.1007/s00281-015-0528-y

Zandstra, T. E., Notenboom, R. G. E., Wink, J., Kiès, P., Vliegen, H. W., Egorova, A. D., Schalij, M. J., De Ruiter, M. C., & Jongbloed, M. R. M. (2021). Asymmetry and Heterogeneity: Part and Parcel in Cardiac Autonomic Innervation and Function. In *Frontiers in Physiology* (Vol. 12). https://doi.org/10.3389/fphys.2021.665298

Zhao, Q., Yu, C. D., Wang, R., Xu, Q. J., Dai Pra, R., Zhang, L., & Chang, R. B. (2022). A multidimensional coding architecture of the vagal interoceptive system. *Nature*, *603*(7903). https://doi.org/10.1038/s41586-022-04515-5

Zhuo, H., Ichikawa, H., & Helke, C. J. (1997). Neurochemistry of the nodose ganglion. *Progress in Neurobiology*, *52*(2). https://doi.org/10.1016/S0301-0082(97)00003-8

Zimmerman, K. D., Espeland, M. A., & Langefeld, C. D. (2021). A practical solution to pseudoreplication bias in single-cell studies. *Nature Communications*, *12*(1). https://doi.org/10.1038/s41467-021-21038-1

Figure Legends

Figure 1. Putative chemosensing and mechanosensing clusters identified in right and left NG in rats. A) Cartoon illustrating pooling of right and left NG from 18 male and 18 female rats into replicate groups. Created in BioRender. Thorn, C. (2024) BioRender.com/w17y601. B) 22 clusters were identified from integrated right and left NG samples. C) All clusters met quality control criteria and expressed high levels of the neuronal marker *Snap25*. D) Clusters can be divided into putative chemosensing (left) versus mechanosensing (right) subtypes based on expression of *Snc10a* and *Oprm1* versus *Scn1a*, *Piezo2*, and *Cntn1*, respectively.

Figure 2. Unique transcript combinations define each NG cluster. A-B) Right vs. left expression of the top 2 cluster-defining genes for each cluster (A) and a select set of genes known to be expressed in NG neurons innervating the heart, lung, and or gut (B).

Figure 3. More *Cckar*-expressing neurons are found in right NG than in left NG. A) Pseudobulk analysis identified 3 clusters with significant right-left differential expression of any genes. B) Differential expression of genes identified in A was generally associated with weak significance levels and/or small effect sizes. C) Percent of cells in each cluster originating from right (R) versus left (L) samples from male (M) vs. female (F) rats. Dashed line denotes percentage of total cells across all clusters obtained from right NG samples. Cluster #5 (cyan arrow) was the only cluster identified as exhibiting significantly greater than expected representation in right NG. *: denotes clusters with significant differential gene expression from (A); F/M: denotes clusters found to have

significantly greater than expected representation in female (F) or male (M) rats; R/L: denotes clusters found to have significantly greater than expected representation in right (R) or left (L) NG. D) Cluster #5 expresses high levels of *Chrna3* and *Cckar*. E) RNA-FISH confirms the presence of a *Cckar*+ (red, row 1) and *Chrna3*+ (blue, row 2) population of neurons (*Snap25*+, green, row 3) in the left and right NG of rats. Merged image (row 4) also shows DAPI-stained nuclei (cyan); scale bars denote 100 μm. F) *Cckar*+ neurons identified using RNA-FISH are significantly more numerous in right NG than in left NG, though no differences are found in the proportions of *Chrna3*+ neurons, or in total number of neurons. *: $p < 0.05$, paired t-test.

Figure 4. Mice also exhibit preferential expression of a *Chrna3*+ and *Cckar*+ subtype in right NG. A) Clustering identified 21 high-quality clusters in the integrated rat + mouse scRNA-seq dataset. B-C) Overlapping UMAP representations (B) and percentages of cells from each dataset distributed across identified clusters (C) indicate rat and mouse data were well integrated. D) In both rat (top) and mouse (bottom) datasets, the *Chrna3*+ and *Cckar*+ cluster, Cluster #6, was identified as having significantly greater than expected representation in samples from the right NG. Dashed lines denotes the percentage of total cells across all clusters obtained from right NG samples in rat (top) and mouse (bottom) datasets.

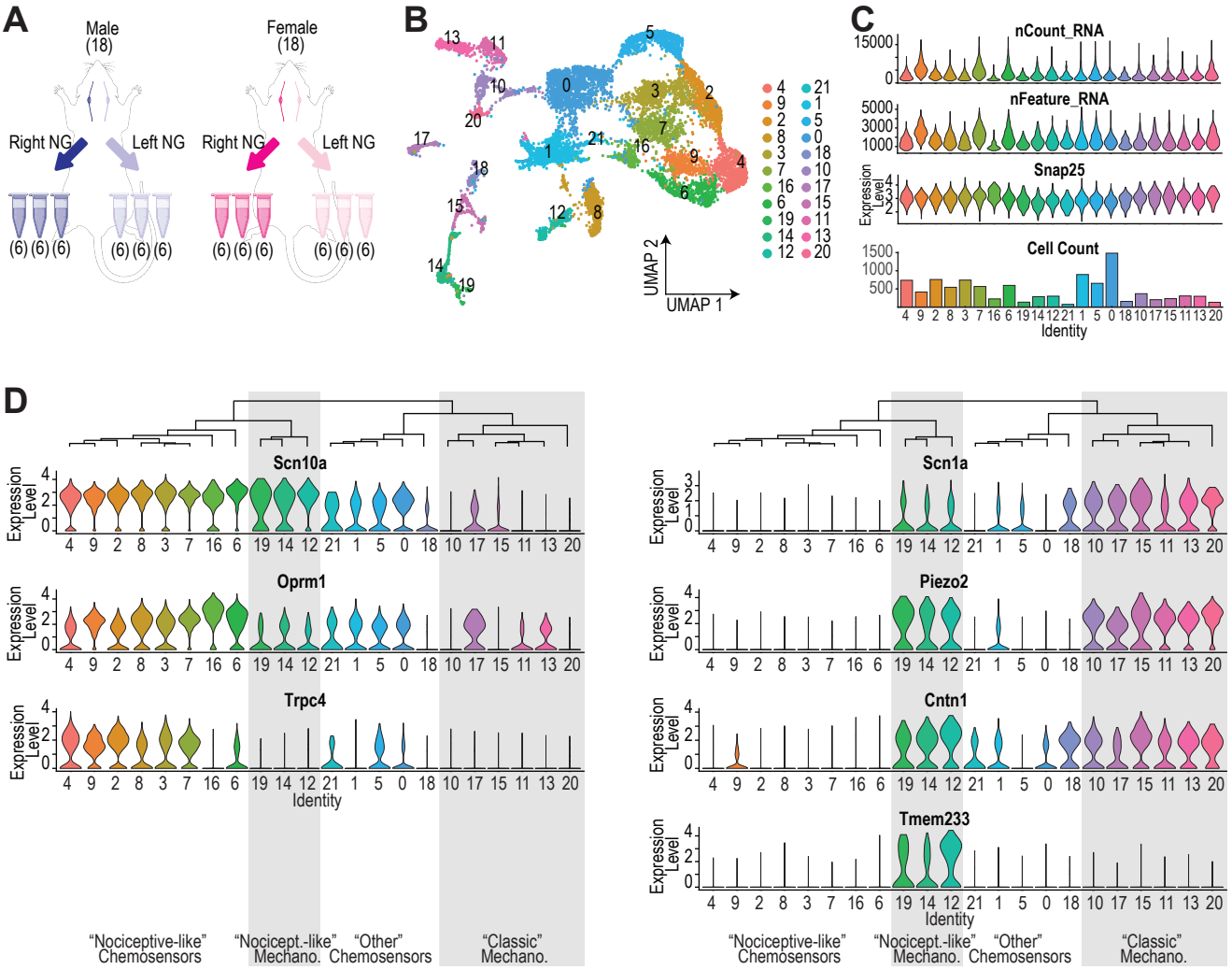
A
Male
(18)
Female
(18)
Right NG
Left NG
Right NG
Left NG
(6) (6) (6)
B
UMAP 2
UMAP 1
C
nCount_RNA
nFeature_RNA
Snap25
Cell Count
Expression Level
Identity
D
Scn10a
Oprm1
Trpc4
Scn1a
Piezo2
Cntn1
Tmem233
Expression Level
Identity
"Nociceptive-like" Chemosensors
"Nocicept.-like" Mechano.
"Other" Chemosensors
"Classic" Mechano.

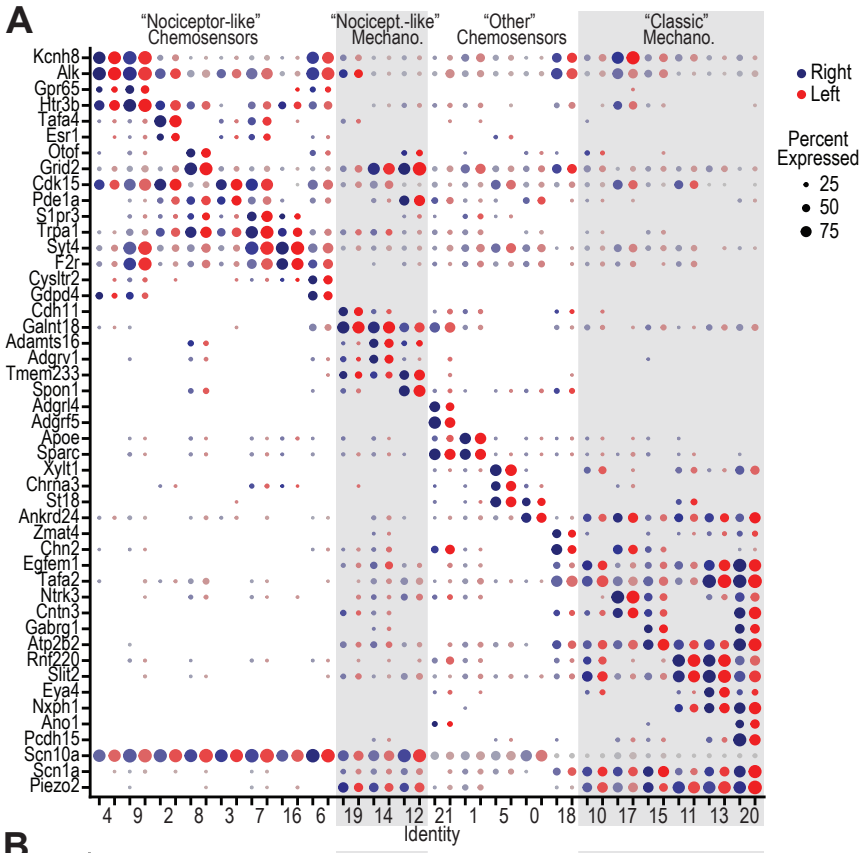
A
"Nociceptor-like" Chemosensors
"Nocicept.-like" Mechano.
"Other" Chemosensors
"Classic" Mechano.
Kcnh8
Alk
Gpr65
Htr3b
Tafa4
Esr1
Otof
Grid2
Cdk15
Pde1a
S1pr3
Trpa1
Syt4
F2r
Cysltr2
Gdpd4
Cdh11
Galnt18
Adamts16
Adgrv1
Tmem233
Spon1
Adgrl4
Adgrf5
Apoe
Sparc
Xylt1
Chrna3
St18
Ankrd24
Zmat4
Chn2
Egfem1
Tafa2
Ntrk3
Cntn3
Gabrg1
Atp2b2
Rnf220
Slit2
Eya4
Nxph1
Ano1
Pcdh15
Scn10a
Scn1a
Piezo2
4 9 2 8 3 7 16 6 19 14 12 21 1 5 0 18 10 17 15 11 13 20
Identity
Right
Left
Percent Expressed
25
50
75

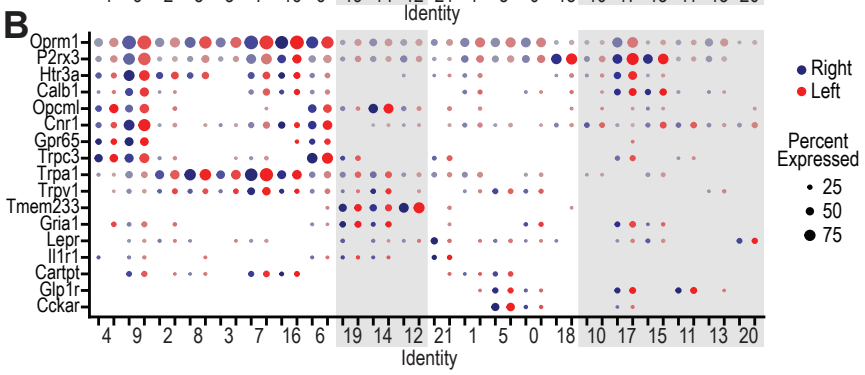
B
Oprm1
P2rx3
Htr3a
Calb1
Opcml
Cnr1
Gpr65
Trpc3
Trpa1
Trpv1
Tmem233
Gria1
Lepr
Il1r1
Cartpt
Glp1r
Cckar
4 9 2 8 3 7 16 6 19 14 12 21 1 5 0 18 10 17 15 11 13 20
Identity
Right
Left
Percent Expressed
25
50
75

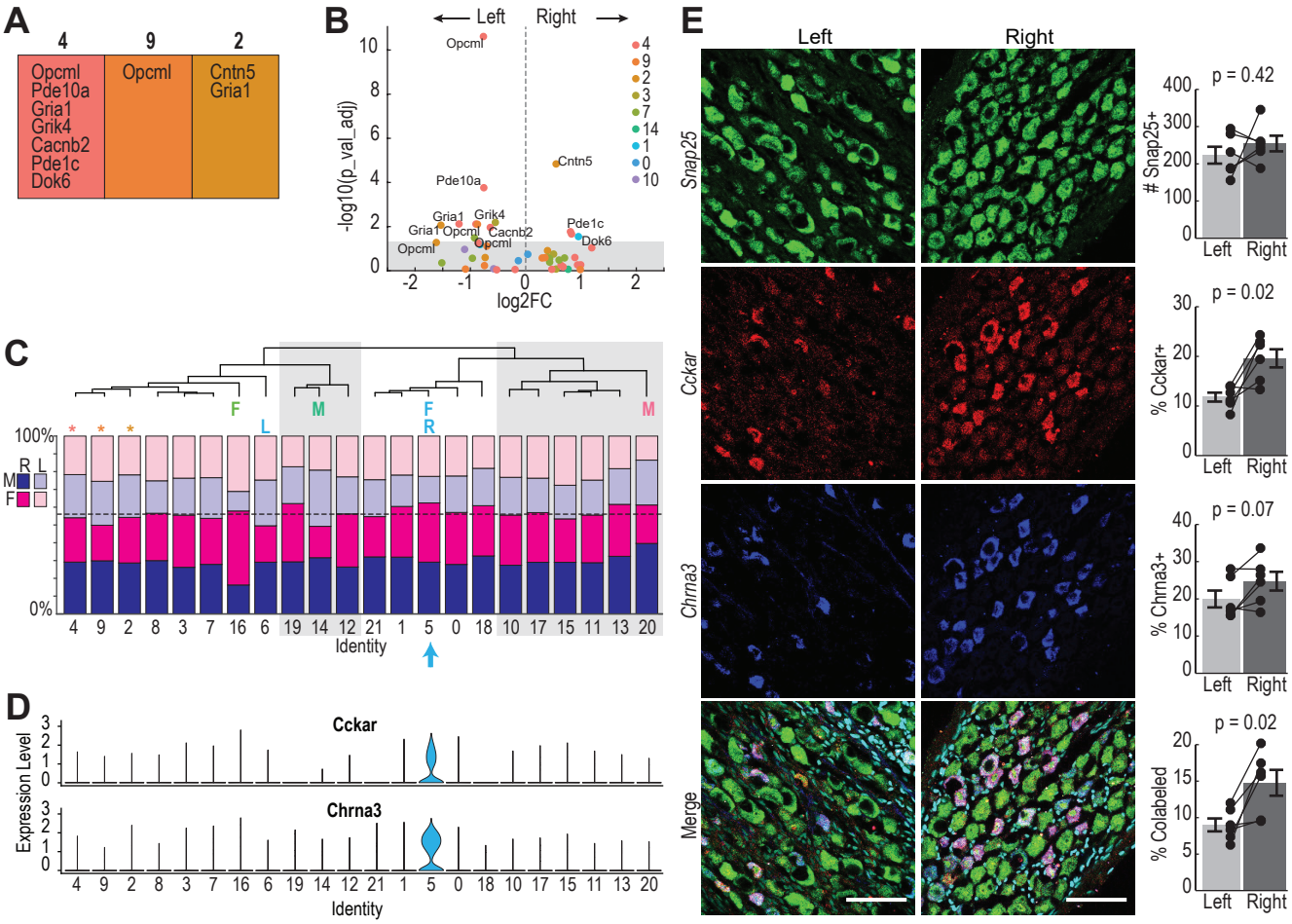
A
4
9
2
Opcml
Pde10a
Gria1
Grik4
Cacnb2
Pde1c
Dok6
Opcml
Cntn5
Gria1
B
Left
Right
-log10(p_val_adj)
log2FC
Opcml
Cntn5
Pde10a
Gria1
Grik4
Gria1
Opcml
Cacnb2
Opcml
Opcml
Pde1c
Dok6
4
9
2
3
7
14
1
0
10
C
F
L
M
F
R
M
100%
0%
R
L
M
F
4 9 2 8 3 7 16 6 19 14 12 21 1 5 0 18 10 17 15 11 13 20
Identity
D
Cckar
Chrna3
Expression Level
4 9 2 8 3 7 16 6 19 14 12 21 1 5 0 18 10 17 15 11 13 20
Identity
E
Left
Right
Snap25
Cckar
Chrna3
Merge
p = 0.42
# Snap25+
Left
Right
p = 0.02
% Cckar+
Left
Right
p = 0.07
% Chrna3+
Left
Right
p = 0.02
% Colabeled
Left
Right

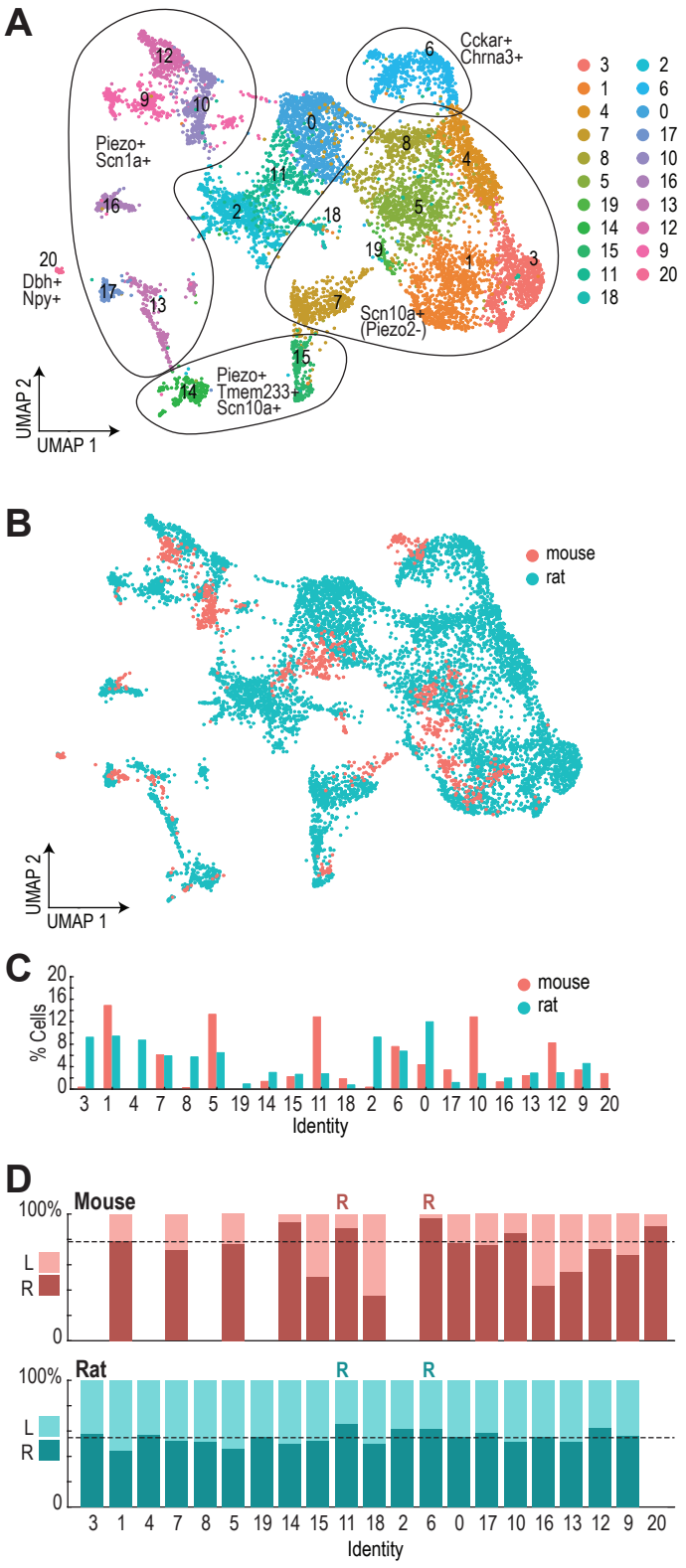
A
Cckar+
Chrna3+
Piezo+
Scn1a+
20
Dbh+
Npy+
Scn10a+
(Piezo2-)
Piezo+
Tmem233+
Scn10a+
UMAP 2
UMAP 1
3 1 4 7 8 5 19 14 15 11 18 2 6 0 17 10 16 13 12 9 20
B
mouse
rat
UMAP 2
UMAP 1
C
% Cells
mouse
rat
Identity
D
Mouse
Rat
L
R
Identity